POLITECNICO DI TORINO
Repository ISTITUZIONALE

Nozaki–Bekki solitons in semiconductor lasers

Original
Nozaki–Bekki solitons in semiconductor lasers / Opacak, N., Kazakov, D., Columbo, L.L., Beiser, M., Letsou, T.P., Pilat, F., Brambilla, M., Prati, F., Piccardo, M., Capasso, F., Schwarz, B.. - In: NATURE. - ISSN 1476-4687. - STAMPA. - 625:7996(2024), pp. 685-690. [10.1038/s41586-023-06915-7]

Availability:
This version is available at: 11583/2990967 since: 2024-09-04T10:15:52Z

Publisher:
Nature Pub.

Published
DOI:10.1038/s41586-023-06915-7

Terms of use:

This article is made available under terms and conditions as specified in the corresponding bibliographic description in the repository

Publisher copyright
GENERICO -- per es. Nature : semplice rinvio dal preprint/submitted, o postprint/AAM [ex default]

The original publication is available at https://www.nature.com/articles/s41586-023-06915-7#rightslink / http://dx.doi.org/10.1038/s41586-023-06915-7.

(Article begins on next page)

15 October 2026

Nozaki-Bekki solitons in semiconductor lasers

Nikola Opačak,[1,2,*] Dmitry Kazakov,[2] Lorenzo L. Columbo,[3] Maximilian Beiser,[1] Theodore P. Letsou,[2,4] Florian Pilat,[1] Massimo Brambilla,[5] Franco Prati,[6] Marco Piccardo,[2,7,8] Federico Capasso,[2] and Benedikt Schwarz[1,2,†]

[1] *Institute of Solid State Electronics, TU Wien, 1040 Vienna, Austria*
[2] *Harvard John A. Paulson School of Engineering and Applied Sciences, Harvard University, Cambridge, MA 02138, USA*
[3] *Dipartimento di Elettronica e Telecomunicazioni, Politecnico di Torino, 10129 Torino, Italy*
[4] *Department of Electrical Engineering and Computer Science, Massachusetts Institute of Technology, Cambridge, MA 02142, USA*
[5] *Dipartimento di Fisica Interateneo and CNR-IFN, Università e Politecnico di Bari, 70125 Bari, Italy*
[6] *Dipartimento di Scienza e Alta Tecnologia, Università dell'Insubria, 22100 Como, Italy*
[7] *Department of Physics, Instituto Superior Técnico, Universidade de Lisboa, 1049-001 Lisbon, Portugal*
[8] *Instituto de Engenharia de Sistemas e Computadores – Microsistemas e Nanotecnologias (INESC MN), 1000-029 Lisbon, Portugal*

Optical frequency comb sources, which emit perfectly periodic and coherent waveforms of light [1], have recently rapidly progressed towards chip-scale integrated solutions. Among them, two classes are particularly significant – semiconductor Fabry-Perót lasers [2–6] and passive ring Kerr microresonators [7–9]. Here we merge the two technologies in a ring semiconductor laser [10, 11] and demonstrate a new paradigm for free-running soliton formation, called Nozaki-Bekki soliton. These dissipative waveforms emerge in a family of traveling localized dark pulses, known within the famed complex Ginzburg-Landau equation [12–14]. We show that Nozaki-Bekki solitons are structurally-stable in a ring laser and form spontaneously with tuning of the laser bias – eliminating the need for an external optical pump. By combining conclusive experimental findings and a complementary elaborate theoretical model, we reveal the salient characteristics of these solitons and provide a guideline for their generation. Beyond the fundamental soliton circulating inside the ring laser, we demonstrate multisoliton states as well, verifying their localized nature and offering an insight into formation of soliton crystals [15]. Our results consolidate a monolithic electrically-driven platform for direct soliton generation and open a door for a new research field at the junction of laser multimode dynamics and Kerr parametric processes.

Dissipative temporal solitons – stable solitary localized pulses – emerge universally in extended nonlinear media, sustained by a dual balance between the nonlinearity and dispersion/diffusion, as well as between the gain and dissipation of the system [16]. Their prime examples in optics came from passively mode-locked lasers [17], optical fibers [18, 19], and passive high-Q microresonators [7, 20]. Being of special interest for integrated photonics due to their compact size, microresonators have taken the community by storm. Fine-tuning of the requisite continuous-wave (CW) optical pump, combined with a bulk Kerr nonlinearity, is necessary to provide the parametric gain that leads to bright or dark microresonator solitons [8, 9, 21]. When outcoupled, the circulating soliton results in a periodic train of short pulses, generating a broad frequency comb in the spectral domain [1]. These miniature Kerr combs have ever since been the vanguard of microresonator technology, finding use in telecommunication [22], ranging [23], high-precision spectroscopy [24], and frequency synthesis [25].

In this work, we demonstrate a new type of optical dissipative solitons – named Nozaki-Bekki (NB) solitons – in an electrically-driven mid-infrared (MIR) ring semiconductor laser. They arise as localized waveforms in a family of traveling dark pulses that satisfy ring periodic boundary conditions. The active laser gain material in our devices simultaneously provides a giant Kerr nonlinearity and eliminates the external optical pump and its challenging frequency tuning, which is a vital ingredient for microresonator combs. The NB soliton regime – first of its kind in a compact optical system – emerges spontaneously and is directly accessed solely by tuning the laser driving current, which we validate by using a phase-sensitive measurement. The experimental findings are corroborated by a complementary theoretical Maxwell-Bloch formalism with numerical simulations, allowing us to identify favourable dispersive and nonlinear conditions for NB soliton formation and their coherent control. Our initial prediction of their existence originated from the cubic complex Ginzburg-Landau equation (CGLE) – one of the most celebrated equations in physics that describes spatially extended systems close to bifurcations [12]. While their stability was long discussed within the CGLE framework, NB solitons have so far been scarcely observed in experiments. Unequivocal classification of NB solitons is made possible by their

* nikola.opacak@tuwien.ac.at
† benedikt.schwarz@tuwien.ac.at

FIG. 1. **Parameter space of the CGLE with corresponding laser regimes.** The unidirectional intracavity intensities and the spectra are obtained from numerical simulations of the CGLE for different points indicated in the parameter space. The left column shows two states triggered by turbulence inside the CW linearly-unstable yellow region of the parameter space (defined by $1 + c_D c_{NL} < 0$), where a single-mode field cannot exist as a steady state. Defect turbulence occurs deep inside the unstable region (point P_1) and is aperiodic, exhibiting chaotic temporal evolution. Close to the border of CW stability (point P_2), phase turbulence leads to narrowband homoclon frequency combs [10]. The right column displays the coexistence (multistability) of a single-mode regime and an NB soliton, both set in the CW linearly-stable part of the parameter space ($1 + c_D c_{NL} > 0$). NB solitons emerge as coherent, unidirectional propagating dark pulses, characterized with a broad and smooth spectral envelope. The visible pulse shoulder represents a shock, stabilizing the waveform in ring periodic boundary conditions.

striking salient characteristics – anti-phase synchronization of the soliton with the primary mode and a 2π temporal phase ramp across the soliton. The localized nature of NB solitons is conclusively demonstrated by further observing multisoliton states, both in theory and experiments. Our findings herald a new generation of monolithically-integrated self-starting soliton generators that lie at the intersection of semiconductor lasers and Kerr microresonators.

To study NB solitons, we use quantum cascade lasers (QCLs) – compact and efficient devices that emit in the MIR and THz regions [26, 27] – embedded in a ring cavity. Ultrafast intersubband transitions of QCLs provide not only the optical gain, but also a giant Kerr nonlinearity [28, 29], which is several orders of magnitude larger than in bulk III-V compounds [30]. This is already exploited for frequency comb formation in Fabry-Pérot (FP) QCLs [2, 6, 28]. There, the multimode operation originates from the spatial hole burning (SHB) [6], which describes inhomogeneous gain saturation due to a standing wave inside the cavity, caused by the counter-propagating components of the electric field. Conversely, a ring cavity has no reflection points and supports unidirectional field propagation – preventing SHB. Nevertheless, recent work demonstrated multimode unidirectional ring QCLs due to phase turbulence at low pumping levels, making SHB nonessential [10]. Since then, substantial efforts were put towards developing Kerr combs in ring QCLs [11, 31, 32], leading even to bright pulses after spectral filtering [33] and theoretically-predicted optically-driven solitons [34, 35] – already anticipating the potential of these devices as an on-chip soliton platform.

We can interpret ring QCL multimode dynamics on the grounds of the CGLE with periodic boundary conditions [10]. Starting from the more general laser master equation [6], we derive the cubic CGLE

$$\partial_t E = E + (1 + ic_D)\partial_z^2 E - (1 + ic_{NL})|E|^2 E, \quad (1)$$

where E is the unidirectional electric field, t is time, and z is the spatial coordinate along the ring cavity (see derivation in the Supplementary material). The entire parameter space is elegantly constricted to just two dimensions, which refer to the dispersive (c_D) and nonlinear effects (c_{NL}). In lasers, c_D is partly determined by the cavity group velocity dispersion (GVD) k''. Another contribution to the total GVD originates from the gain lineshape, defined with the linewidth enhancement factor (LEF) – a crucial semiconductor laser parameter which describes light amplitude-phase coupling [36, 37]. Moreover, the LEF also defines c_{NL} and phenomenologically describes the giant resonant Kerr nonlinearity of QCLs [6, 28]. A linear stability analysis of the CGLE divides the $c_D - c_{NL}$ space in two regions depending on the stability of the single-mode CW solution under small perturbations (Fig. 1) [12]. Deep within the unstable region, defect turbulence occurs, characterized with a broad, unlocked spectrum and chaotically-evolving intracavity intensity (point P_1). Closer to the stable region, the laser undergoes phase turbulence represented by a narrower spectrum and shallow intensity variations (point P_2). Phase turbulence can eventually lead to frequency combs in the form of localized coherent pulse-like structures named homoclons [10, 12].

The stable region of the parameter space sustains single-mode operation. However, we show that multimode emission can exist even here if we allow for large perturbations that are beyond the scope of linear stability analysis. The resulting frequency combs – known as Nozaki-Bekki holes in the CGLE framework [12–14] – have a smooth and broad spectral envelope. In the temporal domain, they correspond to a family of traveling, localized dark pulses that preserve their shape and connect two stable CW fields, giving a constant background. These waveforms exist in a narrow region of the parameter space, and have been so far related to dark solitons [38] and experimentally observed in chemical systems [39], fluids [40], and long-cavity ring lasers [41, 42]. In numerical simulations imposing ring periodic boundary conditions, states comprising an arranged hole and shock pair are structurally-stable even with inclusion of higher-order nonlinear terms that are not accounted for in the cubic CGLE and that play a role in real physical systems e.g. lasers [13, 43, 44]. The coexistence of a stable CW field and a hole-shock pair (point P_3) is a prime example of the phenomenon of multistability – stochastic dependence of the laser state on the starting conditions – thus corroborating the solitonic nature of these dissipative localized structures [7, 16], referred to hereafter as NB solitons in our lasers.

A microscope image of the ring QCL is seen in Fig. 2a), along with an integrated waveguide coupler. The waveguide core is made from the same QCL material and has separate contacts for independent electrical driving. This allows to tune the mode indices, the Q-factor, the power of the extracted light, and the coupling between the waveguide and the ring – making this configuration an

FIG. 2. **Experimental and theoretical characterization of fundamental NB solitons in a monolithic ring laser. a)** Microscope image of the QCL ring and waveguide coupler, with separate electrical contacts. SEM images depict the ring-waveguide coupling region. **b)** Output power of the device as a function of the ring and waveguide currents, J_{R} and J_{WG} respectively. **c)** A narrow optical beatnote of the laser comb at the central frequency of 13.59 GHz, equal to the repetition frequency. **d)** Experimentally-obtained intensity spectrum and the intermode phases of an NB soliton at bias currents of J_{R} =1.33 kA/cm^2 and J_{WG} =0.79 kA/cm^2. Intermode phases between weaker sidemodes are synchronized in-phase, while the phase of the primary mode is π-shifted. Detailed SWIFTS measured data is presented in the Supplementary material. **e)** Temporal profiles of the intensity and phase of the emitted light. Within the width of the NB soliton, the phase changes its value by 2π and remains linear during the remainder of the roundtrip, confirming that the NB soliton is surrounded by a single-frequency constant CW field. **f)** Intensity spectrum obtained from numerical simulations of the master equation, and **g)** zoomed-in top-portion within the same range of 35 dB as the experimental spectrum in d). The π jumps around the primary mode – salient characteristic of NB solitons – are visible in the intermode phases. **h)** The simulated temporal waveforms of the intensity and the phase over two roundtrips. Larger amplitude contrast compared to e) is attributed to the limited dynamic range of detection in experiments, which results in a finite number of spectral modes used for the temporal waveform reconstruction. The simulated NB soliton is obtained for LEF of 1.25, in agreement with typical values in QCLs [37]. The cavity dispersion k'' was set to 800 fs^2/mm, which together with the gain dispersion brings the total GVD value to about -700 fs^2/mm (see Supplementary material for a discussion on different contributions to the effective GVD and nonlinearity in a laser).

ideal testbed for a plethora of resonant electromagnetic phenomena [45]. The light outcoupling in previous experiments relied on the minuscule ring bending losses, thus limiting the extracted power to submilliwatt levels at room temperature [10]. Using the waveguide coupler to efficiently extract the light, our devices reach power levels above 10 mW (Fig. 2b)), bringing them on par with FP QCLs of a similar ridge length and width, fabricated from the same wafer [45]. While the coupling waveguide is biased below the lasing threshold, the ring QCL is driven above it, where it operates in a unidirectional regime after the symmetry-breaking point [33, 45]. We find that at currents partially higher than the lasing threshold J_{th} (around $1.2J_{\mathrm{th}}$), the ring laser emits a multimode field with a narrow beatnote (Fig. 2c)). This implies a high degree of coherence, typical of a frequency comb.

To benchmark comb operation, we employ SWIFTS – an experimental technique that extracts both the amplitude and phase of spectral modes [46]. The measured intensity spectrum (Fig. 2d)) consists of a strong primary mode surrounded by weaker sidemodes that form a smooth envelope, strikingly reminiscent of soliton spectra in microresonators [7–9, 20, 21]. The intermode phases – the phase differences between adjacent modes – are shown below. They are all synchronized in-phase, except around the primary mode, where π jumps indicate destructive interference due to anti-phase synchronization. This is evident from the reconstructed intensity profile (Fig. 2e)), where a single dark pulse circulates around the cavity in an otherwise quasi-constant CW background – consistent with the predicted fundamental NB soliton. Residual intensity oscillations are due to the limited detection bandwidth. Within the width of the NB soliton, the temporal phase exhibits a steep ramp covering 2π and remains linear everywhere else – proving that the CW background around the soliton is constant and contains a single optical frequency equal to that of the primary mode. Similar optical spectra have been observed in Ref. [33] and discussed in relation to passive Kerr combs, however, leaving several open questions on the phyiscal origin, particularly the missing connection to the required bistability, which in passive Kerr combs occurs due to the detuned injected single-mode pump. To corroborate our experimental findings in more detail, we employ numerical simulations of the master equation derived from the Maxwell-Bloch system (Eq. (S2) in the Supplementary material) [6, 28] and identify a new paradigm for free-running soliton formation, called Nozaki-Bekki soliton. The obtained comb spectrum, shown in Fig. 2f), has a smooth spectral envelope engulfing a strong primary mode and spanning over more than 100 cavity modes. Numerical simulations are not constrained by a small dynamical range as the experiment (around 35 dB in Fig. 2d)). Hence, by concentrating on the top part of the simulated spectrum within the same range (Fig. 2g)), we show a clear agreement with the experiment. The simulated intermode phases confirm the π shift between the primary mode and the sidemodes, indicating that this is a hallmark of NB solitons. The simulated temporal intensity in Fig. 2h) matches the structures predicted by the CGLE theory in Fig. 1. In our numerical study, the NB solitons appear to be rather robust against small variations of the dispersive and nonlinear parameters. The soliton width, however, is strongly influenced by the gain bandwidth, which can be analytically shown via a rescaling law (Eq. (S13) Supplementary material). Higher-order dispersion due to the laser gainshape is the likely cause of the residual small ringing that trails the NB soliton, as is well-known from microresonator solitons [47, 48]. The combined simulated and experimental temporal waveforms confirm that NB solitons are surrounded by a CW background – providing a compelling proof of their dissipative soliton nature.

Localization is another striking soliton feature, clearly noticed in multisoliton states – spontaneously ordered ensembles of several co-propagating solitons [7, 8]. Multisoliton states can be indubitably identified by their 'fin-

FIG. 3. **Multisoliton states. a)** Spectral behavior of an experimental multisoliton state, obtained for J_R =1.28 kA/cm^2 and J_{WG} =0.74 kA/cm^2. The interference between two NB solitons causes spectral modulation, resulting in smooth lobes separated by a spectral hole. The intermode phases indicate an additional π jump between the lobes. **b)** Two NB solitons appear in the intensity waveform, surrounded by a CW background. The temporal phase sweeps 4π within the two-soliton region. **c)** Zoomed top portion of the simulated spectrum and the intermode phases, in agreement with a). **d)** The intensity spectrum with the indicated zoomed section, shown in c). The spectral modulation, caused by the interference of the two solitons, cascades through the entire spectrum. **e)** Simulated temporal waveforms of the intensity and the phase. The larger dynamical range compared to the experiment allowed us to distinguish two individual 2π ramps in the phase profile, one for each soliton. The LEF was set to 1.35 and k'' to 600 fs^2/mm (total GVD around -900 fs^2/mm). **f)** Intracavity intensity profiles obtained for the same laser parameters when starting from different random noise conditions, labeled with seed 1,2, and 3. The coexistence of a CW single-mode field, a fundamental NB soliton, and a multisoliton state verifies multistability and the fact that the laser operates in a linearly-stable parameter region. The distance between the NB solitons in a multisoliton state is time-invariant, but it changes for different laser parameters or starting conditions, as is seen from two states in the bottom row. The state in the bottom left is taken from e). Experimental evidence of a soliton crystal, which is a special case of multisoliton states where all of the solitons are equidistant [15], is shown in Extended Data Fig. 1.

FIG. 4. **Coherent control of NB soliton regimes. a)** Spectral shift of the soliton relative to the primary mode as the ring current is swept. Similar behavior is exhibited if the waveguide current is tuned instead. A more detailed SWIFTS characterization is shown in Extended Data Fig. 2. **b)** Sketch of the coupled ring-waveguide system. The bias alters the optical indices of the ring and the waveguide through carrier- and thermal-induced changes, resulting in a mismatch (detailed analysis in the Supplementary material). **c)** Group delay dispersion, calculated with a coupled mode theory analysis, as a function of the index mismatch between the ring and the waveguide, which stems from different bias conditions (Supplementary material). Compared to a single ring cavity, our devices provide superior control of the dispersion. **d)** Simulated soliton spectra as the cavity dispersion k'' is swept, demonstrating a spectral shift of the soliton similar to a). The gainshape contribution to the total GVD is around -1500 fs^2/mm. **e)** Experimentally-obtained intensity spectrum of a NB soliton at bias currents of J_R =1.39 kA/cm^2 and J_{WG} =0.85 kA/cm^2 (red), which corresponds to a bright pulse in the intensity waveform. The soliton sidemodes are stronger compared with the dark-pulse soliton from Fig. 2d) (replotted in blue). **f)** Illustration of the theoretical dependence of the intensity waveform on the soliton spectrum. We assume ideal NB soliton intermode phase distribution with π jumps around the primary mode.

gerprint' optical spectra, which have a modulated envelope due to the interference between individual solitons. Fig. 3a) depicts one such spectrum, consisted of smooth lobes with spectral holes in-between. The intermode phases indicate that, besides the usual π jumps around the primary mode, an additional π jump occurs at the position of the spectral hole – providing another telltale sign of a multisoliton state. The reconstructed intensity (Fig. 3b)) displays two distinct dark pulses, during which the phase changes by 4π – twice as much as for a fundamental NB soliton. Master equation simulations verify multisoliton states as well. The spectral behavior, including the additional π intermode phase jump between the lobes, is seen in Fig. 3c). Other than enabling large amplitude contrast, the dynamic range of simulations allows to resolve the 4π change of the temporal phase in two steps – one for each soliton (Fig. 3e)). Multistability is yet another crucial dissipative soliton trait predicted in Fig. 1. To emulate laser starting from spontaneous emission, weak noise from a random number generator with a defined seed is fed as a starting condition into the master equation (see Methods section). Changing the seed, while keeping other laser parameters fixed, led to three states with different number of solitons (Fig. 3f)). The coexistence of solitons and a single-mode field proves that NB solitons are found in the CW linearly-stable region of the parameter space, as predicted by the CGLE.

Separate electrical contacts of the waveguide and the ring provide two invaluable knobs for soliton control. Demonstrating this, we shift the soliton spectral lobe from red to the blue side of the primary mode purely by tuning the ring current in Fig. 4a). Besides changing the gain and the LEF [10, 28], altering the bias strongly impacts the GVD, as confirmed by a coupled mode theory analysis of the ring-waveguide configuration (Figs. 4b) & c)). A small current-induced index mismatch between the ring and the waveguide induces large changes of the GVD, covering both normal and anomalous values. The key role of GVD is also obvious from numerical simulations in Fig. 4d), where we swept the cavity dispersion. Relative to the primary mode, the soliton is spectrally shifted similarly to Fig. 4a), and in agreement with recent observations in microresonators [21]. More anomalous GVD sets the laser operating point in the linearly-unstable parameter region in analogy to Fig. 1, where neither single-mode nor NB soliton regime can exist. Instead, homoclons form via phase turbulence [10], which we observe both in experiments and simulations (Supplementary material).

Having the possibility to form bright pulses with high peak power would open many doors for NB solitons to be used in nonlinear processes, such as supercontinuum generation [45, 49]. One way of achieving this relies on modifying the phase of the primary mode to remove the destructive interference and induce an intense bright pulse. This could be realized by a second active ring

resonator coupled with the waveguide, acting as a notch filter [50]. Another possibility in this direction is illustrated in Fig. 4e), where we show an NB soliton spectrum (in red), obtained at a larger bias compared to the soliton from Fig. 2 (replotted in blue). Astonishingly, temporal intensity of the former unveils a low-contrast bright pulse. A comparison between the two soliton spectra reveals that the bright one has stronger sidemodes. To gain an intuitive understanding, Fig. 4f) conceptually studies the dependence of the temporal intensity on the corresponding spectrum, while assuming the characteristic intermode phase distribution of NB solitons (see Supplementary material for the full analysis). Whereas the primary mode is fixed, the soliton lobe is gradually increased, with the color coding representing the two states from Fig. 4e). The initial increase of the soliton sidemodes enhances the amplitude contrast of a starting dark pulse, until an intensity equilibrium between the primary mode and the sidemodes is reached. At this point, destructive interference between the background and the soliton is complete and the dark pulse reaches zero at its minimum. Further enhancement of the sidemodes causes a decrease of the pulse amplitude contrast, eventually reaching a quasi-constant waveform despite a broad spectrum, as is also experimentally observed (Supplementary material). Finally, additional sidemode amplification causes the pulse to 'flip over' – resulting in a bright coherent pulse. Both the CGLE and the master equation predict the emergence of NB solitons as dark pulses, however neither of the two treatments takes into account the delayed carrier population response to amplitude modulations [51]. A better understanding of the link between the carrier dynamics and the parametric gain, that is necessary for multimode emission, could allow us to optimize active ring resonators for the emission of high-contrast bright pulses.

In this work, we have demonstrated a new way of direct spontaneous soliton generation by utilizing a MIR semiconductor laser active material implemented in an on-chip integrated ring cavity with a coupler waveguide. The waveguide coupler has an independent bias, ensuring not only higher output powers, but also providing a powerful knob to control the total dispersion of the system. Paired with the giant resonant Kerr nonlinearity of the active material, this solidifies the coupled waveguide-ring configuration as a very fruitful playground for nonlinear phenomena – including the direct generation of electrically-driven NB solitons. The soliton regime is demonstrated by combining both experimental and theoretical results. The number of solitons within one roundtrip varies stochastically with the initial conditions of the lasers. This is indicative of a multistability phenomenon, typical for dissipative solitons in extended systems, paving the way for independent soliton addressing [16].

The spontaneous formation of NB solitons with current tuning, without the need of an external optical pump, makes our QCL rings with coupled waveguides ideal candidates for monolithic soliton generators specifically targeting MIR applications. Even more striking, ring QCL Nozaki-Bekki soliton generators are by design intrinsically feedback-insensitive and do not require optical isolators, which are very challenging to be realized on integrated platforms [52, 53]. This feature comes from the fact that wave propagation inside the ring resonator is unidirectional, and the back-reflected light enters the cavity in the opposite direction. Light propagating in opposite direction is suppressed due to the stronger cross-saturation and only weakly couples to the soliton due to the lack of phase-matching and reflection points in the cavity. This is in strong contrast to frequency-modulated combs from FP lasers, where typically optical isolators are used to prevent the loss of coherence [3, 4, 54]. An experimental comparison is shown in Extended Data Fig. 3 with a more detailed description provided in the Methods section.

Moreover, we predict that NB solitons are not platform-dependent and anticipate their demonstration in other semiconductor laser types, such as the interband cascade- or quantum dot lasers. In any of these laser technologies, the gain material can also be used to realize integrated optical amplifiers and a second ring cavity could be used for spectral filtering of the primary mode. Hence, we propose a master-oscillator-power-amplifier configuration with an in-between spectral filter as an ideal configuration to boost the soliton power and significantly increase the usable comb bandwidth for applications.

[1] T. Udem, R. Holzwarth, and T. W. Hänsch, Optical frequency metrology, Nature **416**, 233 (2002).

[2] A. Hugi, G. Villares, S. Blaser, H. C. Liu, and J. Faist, Mid-infrared frequency comb based on a quantum cascade laser, Nature **492**, 229 (2012).

[3] P. Täschler, M. Bertrand, B. Schneider, M. Singleton, P. Jouy, F. Kapsalidis, M. Beck, and J. Faist, Femtosecond pulses from a mid-infrared quantum cascade laser, Nature Photonics **15**, 919 (2021).

[4] J. Hillbrand, A. M. Andrews, H. Detz, G. Strasser, and B. Schwarz, Coherent injection locking of quantum cascade laser frequency combs, Nature Photonics **13**, 101 (2019).

[5] G. Villares, J. Wolf, D. Kazakov, M. J. Süess, A. Hugi, M. Beck, and J. Faist, On-chip dual-comb based on quantum cascade laser frequency combs, Applied Physics Letters **107** (2015).

[6] N. Opačak and B. Schwarz, Theory of Frequency-Modulated Combs in Lasers with Spatial Hole Burning, Dispersion, and Kerr Nonlinearity, Physical Review Letters **123**, 10.1103/physrevlett.123.243902 (2019).

[7] T. Herr, V. Brasch, J. D. Jost, C. Y. Wang, N. M. Kon-

dratiev, M. L. Gorodetsky, and T. J. Kippenberg, Temporal solitons in optical microresonators, Nature Photonics **8**, 145 (2013).
[8] H. Guo, M. Karpov, E. Lucas, A. Kordts, M. H. P. Pfeiffer, V. Brasch, G. Lihachev, V. E. Lobanov, M. L. Gorodetsky, and T. J. Kippenberg, Universal dynamics and deterministic switching of dissipative Kerr solitons in optical microresonators, Nature Physics **13**, 94 (2016).
[9] X. Xue, Y. Xuan, Y. Liu, P.-H. Wang, S. Chen, J. Wang, D. E. Leaird, M. Qi, and A. M. Weiner, Mode-locked dark pulse Kerr combs in normal-dispersion microresonators, Nature Photonics **9**, 594 (2015).
[10] M. Piccardo, B. Schwarz, D. Kazakov, M. Beiser, N. Opačak, Y. Wang, S. Jha, J. Hillbrand, M. Tamagnone, W. T. Chen, A. Y. Zhu, L. L. Columbo, A. Belyanin, and F. Capasso, Frequency combs induced by phase turbulence, Nature **582**, 360 (2020).
[11] B. Meng, M. Singleton, M. Shahmohammadi, F. Kapsalidis, R. Wang, M. Beck, and J. Faist, Mid-infrared frequency comb from a ring quantum cascade laser, Optica **7**, 162 (2020).
[12] I. S. Aranson and L. Kramer, The world of the complex Ginzburg-Landau equation, Reviews of Modern Physics **74**, 99 (2002).
[13] N. Bekki and K. Nozaki, Formations of spatial patterns and holes in the generalized Ginzburg-Landau equation, Physics Letters A **110**, 133 (1985).
[14] J. Lega, Traveling hole solutions of the complex Ginzburg–Landau equation: a review, Physica D: Nonlinear Phenomena **152-153**, 269 (2001).
[15] M. Karpov, M. H. P. Pfeiffer, H. Guo, W. Weng, J. Liu, and T. J. Kippenberg, Dynamics of soliton crystals in optical microresonators, Nature Physics **15**, 1071 (2019).
[16] N. Akhmediev and A. Ankiewicz, eds., *Dissipative solitons: From optics to biology and medicine* (Springer, 2008).
[17] P. Grelu and N. Akhmediev, Dissipative solitons for mode-locked lasers, Nature Photonics **6**, 84 (2012).
[18] N. Englebert, C. M. Arabí, P. Parra-Rivas, S.-P. Gorza, and F. Leo, Temporal solitons in a coherently driven active resonator, Nature Photonics **15**, 536 (2021).
[19] F. Leo, S. Coen, P. Kockaert, S.-P. Gorza, P. Emplit, and M. Haelterman, Temporal cavity solitons in one-dimensional Kerr media as bits in an all-optical buffer, Nature Photonics **4**, 471 (2010).
[20] M. Rowley, P.-H. Hanzard, A. Cutrona, H. Bao, S. T. Chu, B. E. Little, R. Morandotti, D. J. Moss, G.-L. Oppo, J. S. T. Gongora, M. Peccianti, and A. Pasquazi, Self-emergence of robust solitons in a microcavity, Nature **608**, 303 (2022).
[21] S. Zhang, T. Bi, G. N. Ghalanos, N. P. Moroney, L. D. Bino, and P. Del'Haye, Dark-bright soliton bound states in a microresonator, Physical Review Letters **128**, 10.1103/physrevlett.128.033901 (2022).
[22] P. Marin-Palomo, J. N. Kemal, M. Karpov, A. Kordts, J. Pfeifle, M. H. P. Pfeiffer, P. Trocha, S. Wolf, V. Brasch, M. H. Anderson, R. Rosenberger, K. Vijayan, W. Freude, T. J. Kippenberg, and C. Koos, Microresonator-based solitons for massively parallel coherent optical communications, Nature **546**, 274 (2017).
[23] J. Riemensberger, A. Lukashchuk, M. Karpov, W. Weng, E. Lucas, J. Liu, and T. J. Kippenberg, Massively parallel coherent laser ranging using a soliton microcomb, Nature **581**, 164 (2020).
[24] M.-G. Suh, Q.-F. Yang, K. Y. Yang, X. Yi, and K. J. Vahala, Microresonator soliton dual-comb spectroscopy, Science **354**, 600 (2016).
[25] D. T. Spencer, T. Drake, T. C. Briles, J. Stone, L. C. Sinclair, C. Fredrick, Q. Li, D. Westly, B. R. Ilic, A. Bluestone, N. Volet, T. Komljenovic, L. Chang, S. H. Lee, D. Y. Oh, M.-G. Suh, K. Y. Yang, M. H. P. Pfeiffer, T. J. Kippenberg, E. Norberg, L. Theogarajan, K. Vahala, N. R. Newbury, K. Srinivasan, J. E. Bowers, S. A. Diddams, and S. B. Papp, An optical-frequency synthesizer using integrated photonics, Nature **557**, 81 (2018).
[26] Y. Yao, A. J. Hoffman, and C. F. Gmachl, Mid-infrared quantum cascade lasers, Nature Photonics **6**, 432 (2012).
[27] B. S. Williams, Terahertz quantum-cascade lasers, Nature Photonics **1**, 517 (2007).
[28] N. Opačak, S. D. Cin, J. Hillbrand, and B. Schwarz, Frequency Comb Generation by Bloch Gain Induced Giant Kerr Nonlinearity, Physical Review Letters **127**, 10.1103/physrevlett.127.093902 (2021).
[29] P. Friedli, H. Sigg, B. Hinkov, A. Hugi, S. Riedi, M. Beck, and J. Faist, Four-wave mixing in a quantum cascade laser amplifier, Applied Physics Letters **102**, 222104 (2013).
[30] A. L. Gaeta, M. Lipson, and T. J. Kippenberg, Photonic-chip-based frequency combs, Nature Photonics **13**, 158 (2019).
[31] M. Jaidl, N. Opačak, M. A. Kainz, S. Schönhuber, D. Theiner, B. Limbacher, M. Beiser, M. Giparakis, A. M. Andrews, G. Strasser, B. Schwarz, J. Darmo, and K. Unterrainer, Comb operation in terahertz quantum cascade ring lasers, Optica **8**, 780 (2021).
[32] P. Micheletti, U. Senica, A. Forrer, S. Cibella, G. Torrioli, M. Frankié, J. Faist, M. Beck, and G. Scalari, Thz optical solitons from dispersion-compensated antenna-coupled planarized ring quantum cascade lasers (2022).
[33] B. Meng, M. Singleton, J. Hillbrand, M. Franckié, M. Beck, and J. Faist, Dissipative Kerr solitons in semiconductor ring lasers, Nature Photonics **16**, 142 (2021).
[34] L. Columbo, M. Piccardo, F. Prati, L. Lugiato, M. Brambilla, A. Gatti, C. Silvestri, M. Gioannini, N. Opačak, B. Schwarz, and F. Capasso, Unifying frequency combs in active and passive cavities: Temporal solitons in externally driven ring lasers, Physical Review Letters **126**, 10.1103/physrevlett.126.173903 (2021).
[35] F. Prati, M. Brambilla, M. Piccardo, L. L. Columbo, C. Silvestri, M. Gioannini, A. Gatti, L. A. Lugiato, and F. Capasso, Soliton dynamics of ring quantum cascade lasers with injected signal, Nanophotonics **10**, 195 (2020).
[36] C. Henry, Theory of the linewidth of semiconductor lasers, IEEE Journal of Quantum Electronics **18**, 259 (1982).
[37] N. Opačak, F. Pilat, D. Kazakov, S. D. Cin, G. Ramer, B. Lendl, F. Capasso, and B. Schwarz, Spectrally resolved linewidth enhancement factor of a semiconductor frequency comb, Optica **8**, 1227 (2021).
[38] N. Efremidis, K. Hizanidis, H. E. Nistazakis, D. J. Frantzeskakis, and B. A. Malomed, Stabilization of dark solitons in the cubic Ginzburg-Landau equation, Physical Review E **62**, 7410 (2000).
[39] J.-J. Perraud, A. D. Wit, E. Dulos, P. D. Kepper, G. Dewel, and P. Borckmans, One-dimensional "spirals": Novel asynchronous chemical wave sources, Physical Review Letters **71**, 1272 (1993).
[40] J. Burguete, H. Chaté, F. Daviaud, and N. Mukolobwiez,

Bekki-Nozaki Amplitude Holes in Hydrothermal Nonlinear Waves, Physical Review Letters **82**, 3252 (1999).
[41] S. Slepneva, B. O'Shaughnessy, A. G. Vladimirov, S. Rica, E. A. Viktorov, and G. Huyet, Convective Nozaki-Bekki holes in a long cavity OCT laser, Optics Express **27**, 16395 (2019).
[42] U. Gowda, A. Roche, A. Pimenov, A. G. Vladimirov, S. Slepneva, E. A. Viktorov, and G. Huyet, Turbulent coherent structures in a long cavity semiconductor laser near the lasing threshold, Optics Letters **45**, 4903 (2020).
[43] S. Popp, O. Stiller, I. Aranson, A. Weber, and L. Kramer, Localized hole solutions and spatiotemporal chaos in the 1D complex Ginzburg-Landau equation, Physical Review Letters **70**, 3880 (1993).
[44] S. Popp, O. Stiller, I. Aranson, and L. Kramer, Hole solutions in the 1D complex Ginzburg-Landau equation, Physica D: Nonlinear Phenomena **84**, 398 (1995).
[45] D. Kazakov, T. P. Letsou, M. Beiser, Y. Zhi, N. Opačak, M. Piccardo, B. Schwarz, and F. Capasso, Semiconductor ring laser frequency combs with active directional couplers (2022).
[46] D. Burghoff, Y. Yang, D. J. Hayton, J.-R. Gao, J. L. Reno, and Q. Hu, Evaluating the coherence and time-domain profile of quantum cascade laser frequency combs, Optics Express **23**, 1190 (2015).
[47] J. K. Jang, M. Erkintalo, S. G. Murdoch, and S. Coen, Observation of dispersive wave emission by temporal cavity solitons, Optics Letters **39**, 5503 (2014).
[48] M. H. Anderson, W. Weng, G. Lihachev, A. Tikan, J. Liu, and T. J. Kippenberg, Zero dispersion Kerr solitons in optical microresonators, Nature Communications **13**, 10.1038/s41467-022-31916-x (2022).
[49] E. Obrzud, S. Lecomte, and T. Herr, Temporal solitons in microresonators driven by optical pulses, Nature Photonics **11**, 600 (2017).
[50] D. Liu, L. Zhang, Y. Tan, and D. Dai, High-order adiabatic elliptical-microring filter with an ultra-large free-spectral-range, Journal of Lightwave Technology **39**, 5910 (2021).
[51] T. S. Mansuripur, C. Vernet, P. Chevalier, G. Aoust, B. Schwarz, F. Xie, C. Caneau, K. Lascola, C. en Zah, D. P. Caffey, T. Day, L. J. Missaggia, M. K. Connors, C. A. Wang, A. Belyanin, and F. Capasso, Single-mode instability in standing-wave lasers: The quantum cascade laser as a self-pumped parametric oscillator, Physical Review A **94**, 10.1103/physreva.94.063807 (2016).
[52] A. D. White, G. H. Ahn, K. V. Gasse, K. Y. Yang, L. Chang, J. E. Bowers, and J. Vučković, Integrated passive nonlinear optical isolators, Nature Photonics **17**, 143–149 (2022).
[53] C. Xiang, W. Jin, O. Terra, B. Dong, H. Wang, L. Wu, J. Guo, T. J. Morin, E. Hughes, J. Peters, Q.-X. Ji, A. Feshali, M. Paniccia, K. J. Vahala, and J. E. Bowers, 3D integration enables ultralow-noise isolator-free lasers in silicon photonics, Nature **620**, 78–85 (2023).
[54] G. Villares, A. Hugi, S. Blaser, and J. Faist, Dual-comb spectroscopy based on quantum-cascade-laser frequency combs, Nature Communications **5**, 10.1038/ncomms6192 (2014).

METHODS

Feedback-insensitive comb generation. Delayed optical feedback is a major issue in QCL frequency comb applications. It destabilizes the laser output and impacts the nonlinear dynamics and coherence of the frequency comb state [4]. Using optical isolators is one of the most common methods to prevent optical feedback. They must be employed in free-space tabletop systems, such as QCL-based dual-comb spectrometers and external pulse compressors [3, 54]. Downscaling these systems to integrated photonic chips requires alternative methods to mitigate the effects of back-reflections from the downstream components [52, 53]. Here we show that ring QCL Nozaki-Bekki soliton generators are by design, intrinsically feedback-insensitive. This feature comes from the fact that wave propagation inside the ring resonator occurs only in one direction, and the back-reflected light enters the cavity in the opposite direction. As the gain is strongly saturated by the unidirectional laser field, the back-reflected wave quickly dies out inside of the resonator after entering it, having minimal effect on the dynamics of the laser field. In a Fabry-Perot laser the field is bidirectional, and will experience cross-gain saturation from the back-reflected radiation, destabilizing the laser state. It can be very clearly observed from the spectrogram of the intermode beat note of such a Fabry-Perot frequency comb subject to delayed optical feedback (Fig. **3a**). The beat note loses coherence and experiences strong fluctuations for a wide range of feedback intensities. Ring QCLs generating unidirectional Nozaki-Bekki solitons are free of feedback-induced instabilities. The beat note in the ring QCL remains coherent throughout the entire range of back-reflected intensities (Fig. **3b**). This fundamental feature makes ring QCLs potential rivals of Fabry-Perot QCL combs in spectroscopy applications, especially for integrated solutions, such as on-chip dual-comb spectrometers [5].

Device fabrication and operation. The QCLs emit at around 8.2 µm and consist of GaInAs/AlInAs layers on an InP substrate, with the band structure design based on a standard single-phonon continuum depopulation scheme. The waveguides and the narrow gap in the coupling region are etched using the standard fabrication recipe employing optical lithography. The waveguide width is 10 mm, the curved section of the racetrack is a semicircle with a radius of 500 µm, and the length of the straight section is 1.5 mm. The ring circumference defines the cavity repetition rate of around 13.6 GHz. The heat sink temperature was kept at 14°C in all experiments.

Experimental setup and characterisation of the soliton states. The measurement of the spectral amplitudes and phases, that are used for the reconstruction of the temporal waveform, is done by utilizing

the SWIFTS technique [46]. An overview of the measurement procedure is in the Supplementary material. In order to record the laser output modulation at the repetition frequency, we employ a 50 GHZ quantum well infrared photodetector cooled to 77 K, originally purchased from Debut Optoelectronics together with a bias-tee and a low-noise RF preampliferer. For beam collimation we used a 8-12 µm AR coated aspheric BD-2 lens with f=3 mm and NA=0.71 mounted on a high precision 3-axis flexure stage from Thorlabs. The setup uses a custom-built high-resolution Fourier transform infrared (FTIR) spectrometer (∼500 MHz). A Zurich Instruments UHFLI lock-in amplifier is used for the acquisition of both the intensity and SWIFTS interferograms. In order to stabilize the repetition frequency of the comb, we rely on electrical injection locking via a radio-frequency (RF) source. However, caution is required since using a too large injection power will perturb the soliton spectrum and its intermode phases, as can be seen in the Supplementary material. The light that is generated in and outcoupled from QCLs is TM-polarized due to the selection rules of intersubband transitions within the conduction band.

Numerical simulations. Simulations of the CGLE are implemented using a pseudo-spectral algorithm coupled with an exponential time-differencing scheme. The master equation of a unidirectional field is discretized with a first-order forward finite difference method. This method hugely benefits from parallel implementation on a graphics processing unit (GPU), cutting down the execution time by 3 orders of magnitude compared to a standard implementation on the central processing unit. As an example, we simulate tens of millions of time steps within minutes using an NVIDIA GeForce RTX 3070 GPU (tens of thousands of simulated cavity roundtrips are necessary to ensure that a steady state is obtained). To emulate a laser starting from spontaneous emission, the numerical simulations are run with random weak intensity noise as a starting condition obtained from a random number generator with a defined seed value. Changing the seed results in a different randomly generated weak waveform, while preserving the mean intensity and variance. Weak noise is also added in the same way at every discretized cavity grid point after each time step.

ACKNOWLEDGEMENTS

This project has received funding from the European Research Council (ERC) under the European Union's Horizon 2020 research and innovation programme (Grant agreement No. 853014), and from the National Science Foundation under Grant No. ECCS-2221715. T. P. L. would like to thank the support of the Department of Defense (DoD) through the National Defense Science and Engineering Graduate (NDSEG) Fellowship Program.

AUTHOR CONTRIBUTIONS

N. Opačak, D. Kazakov, F. Pilat, T. P. Letsou, and B. Schwarz carried out the experiments and analyzed the data. M. Beiser fabricated the device. N. Opačak performed the master equation simulations. L. L. Columbo, M. Brambilla, and F. Prati did the CGLE simulations and contributed to the analysis of the experimental results and their interpretation in the framework of the CGLE theory. N. Opačak prepared the manuscript with input from all coauthors. N. Opačak, T. P. Letsou, D. Kazakov, and F. Pilat wrote sections of the Supplementary material. B. Schwarz, M. Piccardo, and F. Capasso supervised the project. All authors contributed to the discussion of the results.

COMPETING INTERESTS

The authors declare no competing interests

DATA AND CODE AVAILABILITY

Source data for Figs. 1–4 are provided with the paper. Additional data that support the findings of this study are available from the corresponding authors upon reasonable request.

CODE AVAILABILITY

Information on the code developed to simulate the QCL dynamics and its results are available from the corresponding authors upon reasonable request.

CORRESPONDENCE

Correspondence and requests for materials should be addressed to N. Opačak or B. Schwarz.

Extended data Fig. 1. **Experimental evidence suggesting an NB soliton crystal.** Intensity spectrum of a probable fifth harmonic frequency comb, where the intermode spacing equals 5 FSRs. The soliton crystal regime is suggested by the smooth bell-shaped envelope of the spectrum. In the Fig. 3 of the main manuscript, we have shown an experimental and theoretical characterization of a multisoliton state comprised of two co-propagating NB solitons in a single roundtrip. A special case of multisolitonic states, where all of the solitons within one roundtrip are equidistant, is called a soliton crystal [15]. In the frequency domain, these waveforms correspond to a harmonic frequency comb whose spacing between adjacent comb modes is equal to an integer multiple of the FSR: N $\times$ FSR, where N is the number of solitons in the soliton crystal. The coherence of the state is suggested by the high suppression ratio of the fundamental modes that fall beneath the noise floor, leaving only the harmonic equidistant modes. Furthermore, the modes form a smooth bell-shaped spectral envelope that indicates the soliton nature of the state. The high frequency of the intermode beatnote (around 68 GHz) lies well above the cutoff frequency of our optical detector, thus prohibiting SWIFTS characterization to truly assess the coherence of the state. This begs for the future use of another coherent technique to study soliton crystal dynamics in active ring resonators.

Extended data Fig. 2. **Shifting of the soliton spectral envelope relative to the primary mode.** Experimental characterization of two NB solitons where the tuning of the bias current results in a shift of the spectral soliton envelope from the red to the blue side of the primary mode (**a** and **b** respectively). The shift of the soliton spectral envelope happens as the currents of the ring and the waveguide are changed. The main reason for this likely lies in the large change of the total GVD, as discussed in the main manuscript, and recently observed experimentally in passive microresonators [21]. Although the soliton envelope may be positioned differently relative to the primary mode, the expected two π jumps of the intermode phases around the primary mode are still present – indicating that this is indeed a salient feature of NB solitons. The temporal profile of the phase exhibits the familiar 2π ramp within the width of the soliton. We can observe that the direction of the ramp depends on whether the soliton spectral envelope is on the red or on the blue side relative to the primary mode. In a hypothetical state where the soliton envelope would be perfectly symmetric relative to the primary mode (if the soliton spectral center of mass coincides with the position of the primary mode), the 2π phase ramp would comprise two separate π ramps with an opposite direction. However, this state does not represent a stable fixed point, and is likely never to occur experimentally.

Extended data Fig. 3. **Laser operation under delayed optical feedback.** **a**, Fabry-Perot QCL spectrogram of the intermode beat note under delayed feedback induced by placing a mirror at the laser output. The feedback intensity is varied by rotating a polarizer placed between the laser facet and the mirror. The frequency axis of the spectrogram is centered at 5.833 GHz. **b**, Same measurement as in **a**, performed on a ring QCL generating a unidirectional Nozaki-Bekki soliton. The frequency axis of the spectrogram is centered at 18.623 GHz. In both measurements resolution bandwidth of the RF spectrum analyzer is 16 kHz.

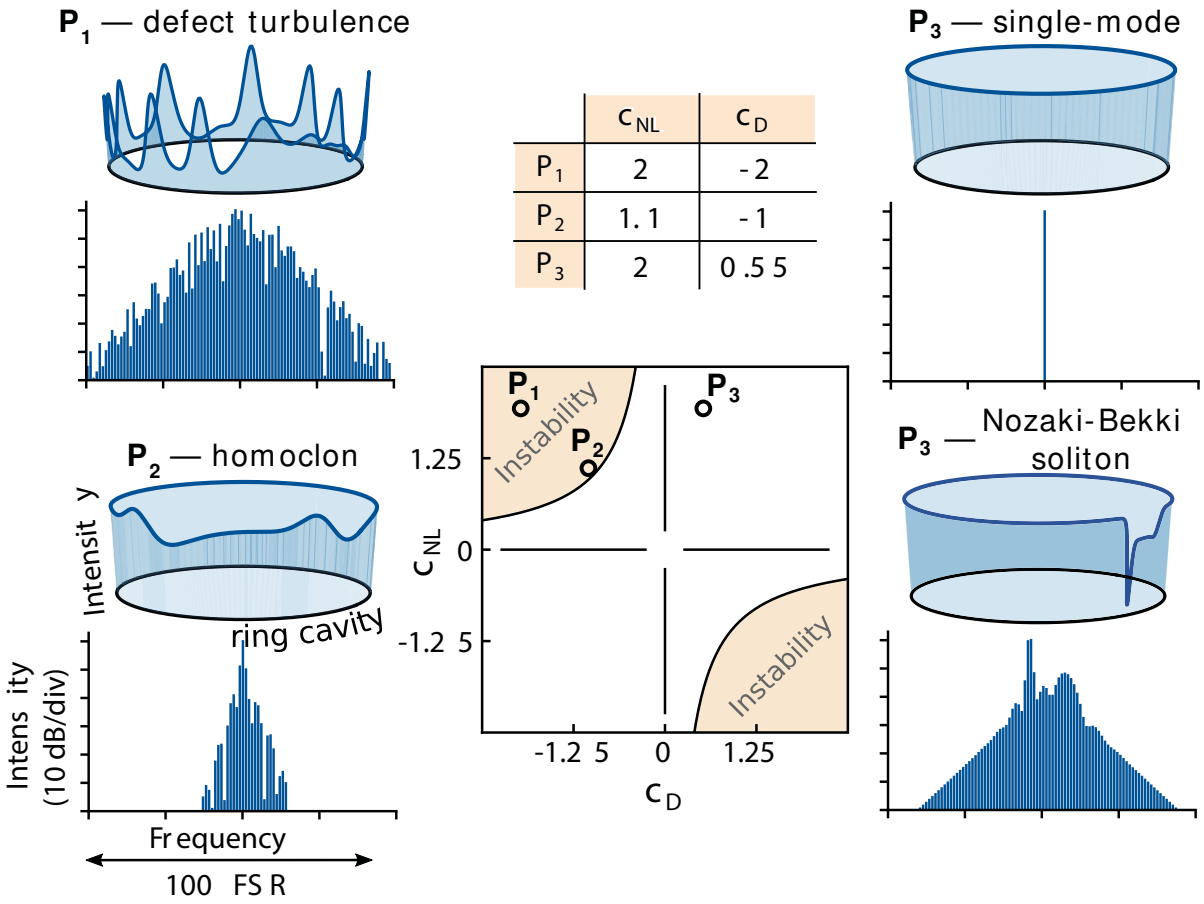

	c_{NL}	c_D
P_1	2	-2
P_2	1.1	-1
P_3	2	0.55

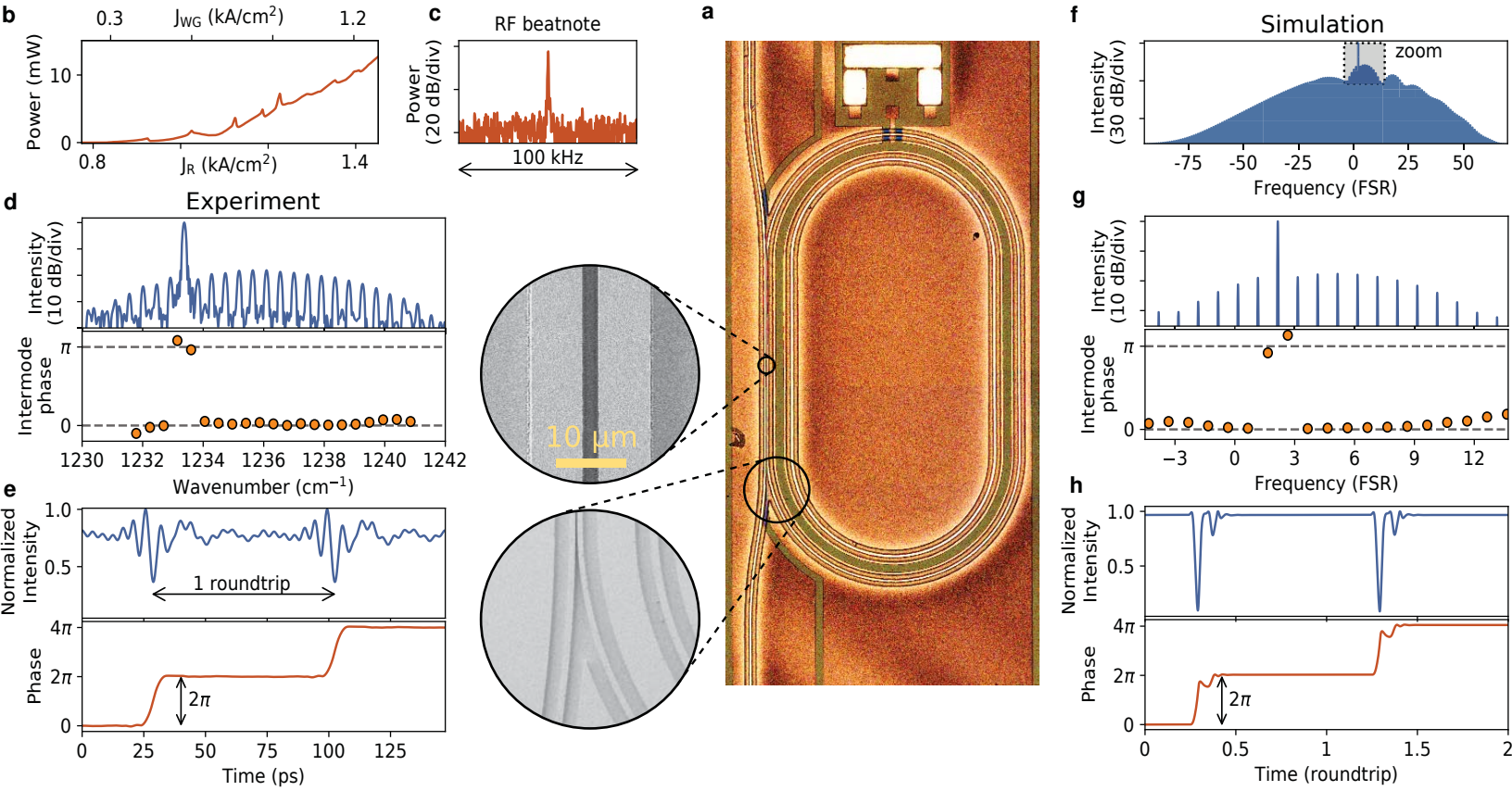
b
0.3
J_{WG} (kA/cm^2)
1.2
Power (mW)
10
0
0.8
J_R (kA/cm^2)
1.4
c
RF beatnote
Power
(20 dB/div)
100 kHz
a
10 μm
f
Simulation
Intensity
(30 dB/div)
zoom
-75
-50
-25
0
25
50
Frequency (FSR)
d
Experiment
Intensity
(10 dB/div)
Intermode
phase
π
0
1230
1232
1234
1236
1238
1240
1242
Wavenumber (cm^{-1})
g
Intensity
(10 dB/div)
Intermode
phase
π
0
−3
0
3
6
9
12
Frequency (FSR)
e
Normalized
Intensity
1.0
0.5
1 roundtrip
Phase
4π
2π
0
2π
0
25
50
75
100
125
Time (ps)
h
Normalized
Intensity
1.0
0.5
Phase
4π
2π
0
2π
0
0.5
1
1.5
2
Time (roundtrip)

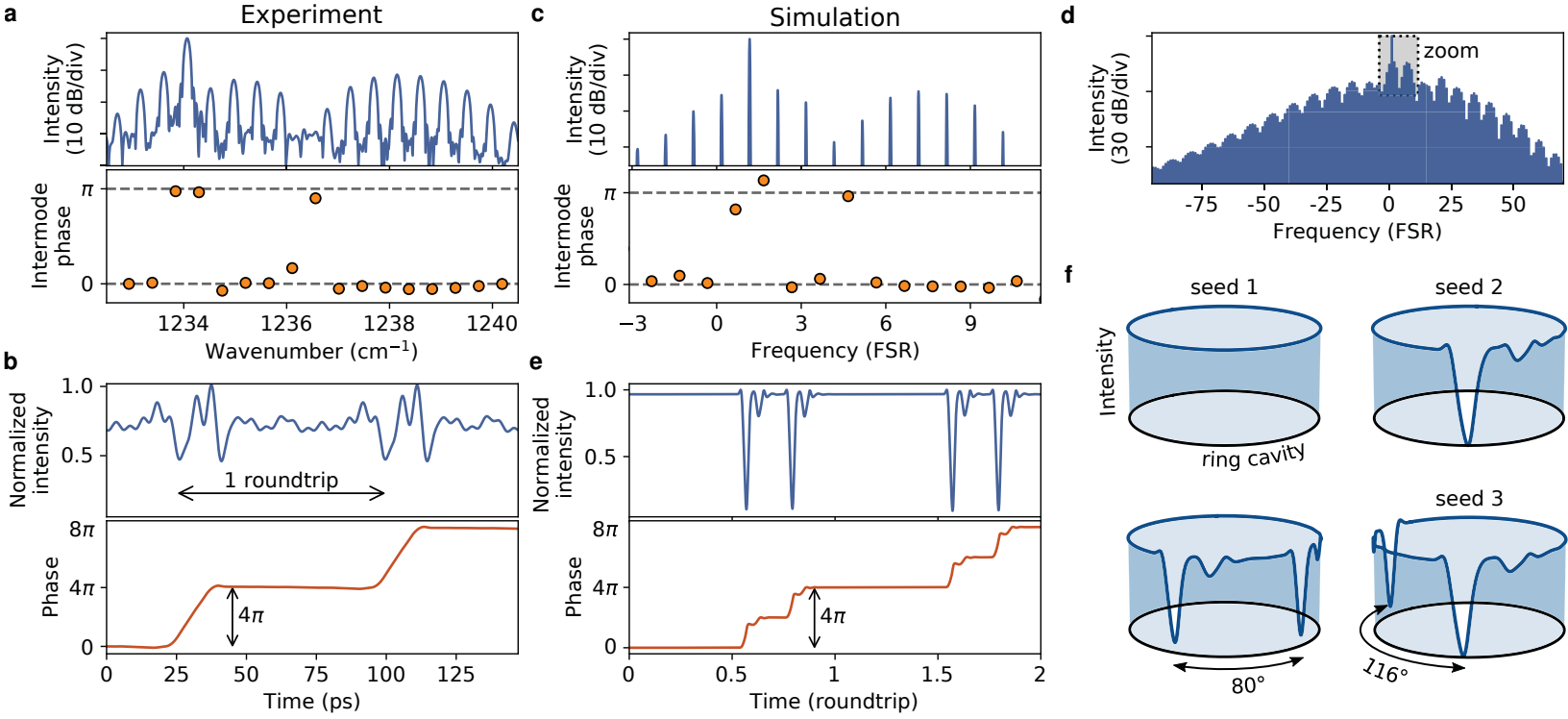
a
Experiment
Intensity (10 dB/div)
Intermode phase
π
0
1234
1236
1238
1240
Wavenumber (cm^{-1})
b
Normalized intensity
1.0
0.5
1 roundtrip
Phase
8π
4π
0
4π
0
25
50
75
100
125
Time (ps)
c
Simulation
Intensity (10 dB/div)
Intermode phase
π
0
−3
0
3
6
9
Frequency (FSR)
e
Normalized intensity
1.0
0.5
Phase
8π
4π
0
4π
0
0.5
1
1.5
2
Time (roundtrip)
d
Intensity (30 dB/div)
zoom
-75
-50
-25
0
25
50
Frequency (FSR)
f
seed 1
seed 2
Intensity
ring cavity
seed 3
80°
116°

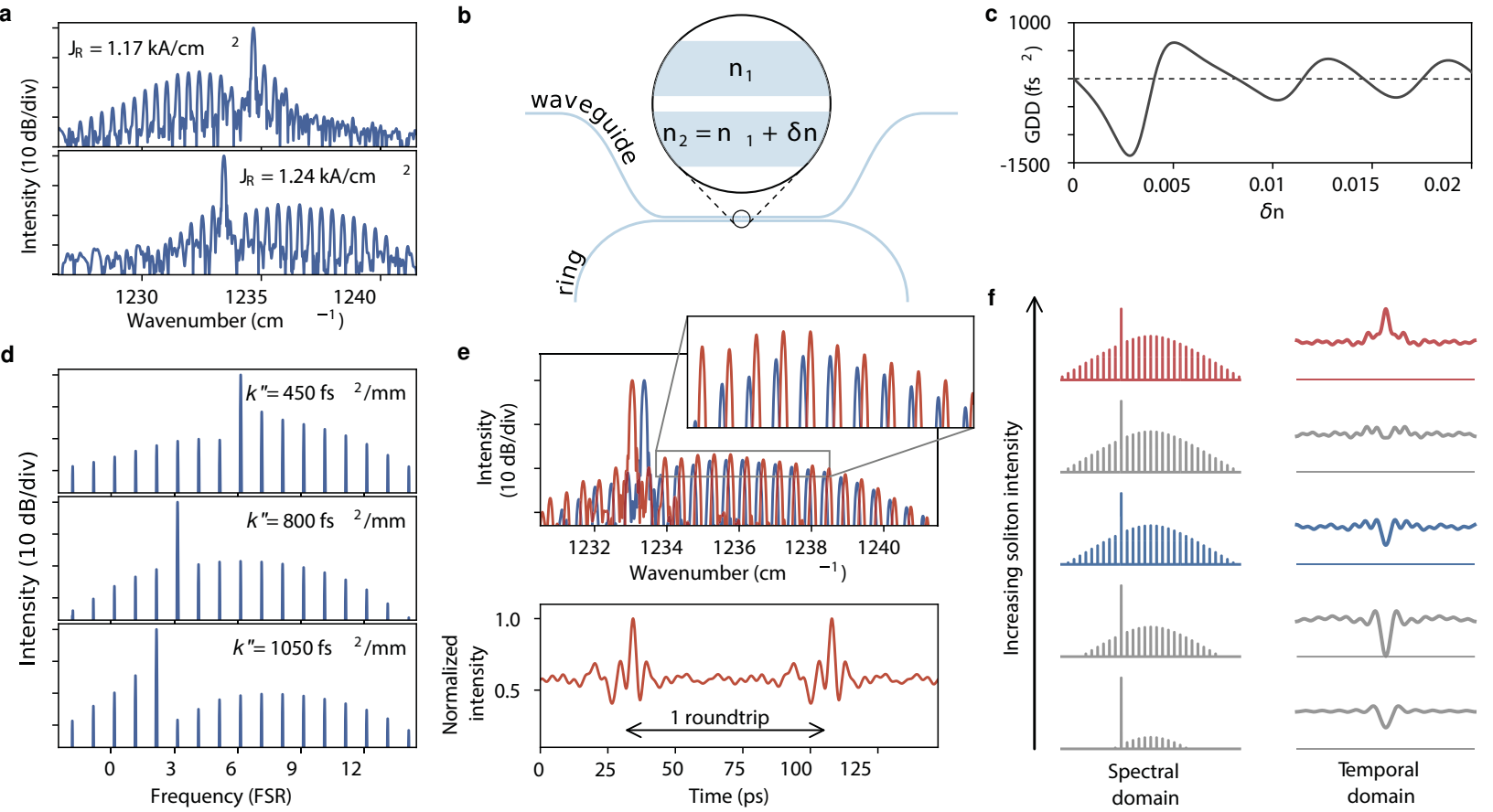
a
J_R = 1.17 kA/cm^2
J_R = 1.24 kA/cm^2
Intensity (10 dB/div)
1230
1235
1240
Wavenumber (cm^{-1})
b
waveguide
ring
n_1
$n_2 = n_1 + \delta n$
c
1000
-1500
GDD (fs^2)
0
0.005
0.01
0.015
0.02
δn
d
k''= 450 fs^2/mm
k''= 800 fs^2/mm
k''= 1050 fs^2/mm
Intensity (10 dB/div)
0
3
6
9
12
Frequency (FSR)
e
Intensity (10 dB/div)
1232
1234
1236
1238
1240
Wavenumber (cm^{-1})
Normalized intensity
1.0
0.5
1 roundtrip
0
25
50
75
100
125
Time (ps)
f
Increasing soliton intensity
Spectral domain
Temporal domain